

## Journal Pre-proof

In-vitro prediction of the membranotropic action of emerging organic contaminants using a liposome-based multidisciplinary approach

Miquel Oliver, Miquel Adrover, Antonio Frontera, Joaquín Ortega-Castro, Manuel Miró



PII: S0048-9697(20)33616-0

DOI: <https://doi.org/10.1016/j.scitotenv.2020.140096>

Reference: STOTEN 140096

To appear in: *Science of the Total Environment*

Received date: 15 April 2020

Revised date: 4 June 2020

Accepted date: 7 June 2020

Please cite this article as: M. Oliver, M. Adrover, A. Frontera, et al., In-vitro prediction of the membranotropic action of emerging organic contaminants using a liposome-based multidisciplinary approach, *Science of the Total Environment* (2020), <https://doi.org/10.1016/j.scitotenv.2020.140096>

This is a PDF file of an article that has undergone enhancements after acceptance, such as the addition of a cover page and metadata, and formatting for readability, but it is not yet the definitive version of record. This version will undergo additional copyediting, typesetting and review before it is published in its final form, but we are providing this version to give early visibility of the article. Please note that, during the production process, errors may be discovered which could affect the content, and all legal disclaimers that apply to the journal pertain.

© 2020 Published by Elsevier.

## ***In-vitro* prediction of the membranotropic action of emerging organic contaminants using a liposome-based multidisciplinary approach**

Miquel Oliver<sup>a</sup>, Miquel Adrover<sup>b</sup>, Antonio Frontera<sup>c</sup>, Joaquín Ortega-Castro<sup>b</sup>, Manuel Miró<sup>a\*</sup>

a) FI-TRACE group, Department of Chemistry, University of the Balearic Islands, Carretera de Valldemossa km 7.5, E-07122 Palma de Mallorca, Spain.

b) REACMOL group, Department of Chemistry, University of the Balearic Islands, Carretera de Valldemossa km 7.5, E-07122 Palma de Mallorca, Spain.

c) SUPRAMOL group, Department of Chemistry, University of the Balearic Islands, Carretera de Valldemossa km 7.5, E-07122 Palma de Mallorca, Spain.

### **Abstract**

According to ISO 17402:2008 more knowledge is needed on processes controlling bioavailability of organic species so as to close the still existing gap between chemical measurements and biological effects. The bioavailability concept encompasses the investigation of the degree of penetration of target species across biological membranes. In addition, REACH (Registration, Evaluation, Authorisation and restriction of Chemicals) guidelines promote the use of *in-vitro* methods against conventional ecotoxicological tests because of the ethical controversy of *in-vivo* tests. This work is aimed at filling the gap by proposing a multidisciplinary approach based on high-resolution and low-resolution empirical techniques, and theoretical quantum mechanics for the *in-vitro* investigation of the bioavailability and membranotropic effects of organic emerging contaminants, including bioaccumulation, via passive diffusion across lipid bilayers. Phosphatidylcholine (PC) liposomes are selected as biomembrane surrogates, and contaminant effects are explored by (i) fluorescence anisotropy and generalized polarization assays using membrane fluorescence probes (laurdan and prodan) and UV-Vis spectroscopy, (ii) <sup>1</sup>H NMR measurements to ascertain supramolecular interactions with PC and (iii) molecular dynamics simulations. In particular, un-regulated model compounds with distinct physico-chemical properties that are representative of three different classes of emerging contaminants in environmental compartments are chosen for validation of the holistic approach: (i) diclofenac as a model of anti-inflammatory drug; (ii) triclosan as an anti-microbial

\* Corresponding author: Manuel Miró (manuel.miro@uib.es)

agent; and (iii) bisphenol A as a plastic additive, and compared with chlorpyrifos as a legacy insecticide. Laurdan anisotropic measurements are in good agreement with  $^1\text{H}$  NMR data and both approaches pinpoint that triclosan and chlorpyrifos are highly bioaccumulable in membranes. Molecular dynamic studies indicate that the lateral diffusion of the lipid bilayer is much lower with the incorporation of either triclosan and chlorpyrifos into the bilayer. The theoretical simulations also allowed estimating absolute bioavailability data under passive diffusion (< 0.1%, 63%, 73% and 89% for diclofenac, bisphenol A, triclosan and chlorpyrifos, respectively) given as the percentage of time that a given species is located in the region of the fatty acyl chains.

Our findings indicate that PC-based liposome assays serve as a fast and cost-effective in-vitro approach, notwithstanding its low resolution features, for environmental bioavailability studies of emerging contaminants for which insufficient or inconsistent ecotoxicological data are identified in the literature.

**Keywords:** bioavailability, liposome, lipid bilayer, emerging contaminants, membrane, permeability

## Introduction

Industrial developments are linked to the launching of novel objects that impact our daily life. To ameliorate their shelf time, organic chemicals with given physicochemical properties, such as anti-microbials, preservatives, nanomaterials, and additives have been introduced in the market, in some instances, for replacing banned compounds. Other chemicals such as pharmaceuticals and personal care products including anti-inflammatory drugs, anti-diabetics, antibiotics, cosmetics, UV-sunscreens and fragrances<sup>1</sup> have been continuously used since decades to serve for human well-being. Recent studies have however demonstrated that most of these compounds are environmentally persistent chemicals, and in some cases, inefficiently removed by wastewater treatment plants or biodegradation processes.<sup>2,3</sup> Also, they might have adverse effects against the ecosystem services and the quality of aquatic biota.<sup>4</sup>

The term ‘*contaminants of emerging concern*’ or ‘*emerging contaminants*’ is actually coined to refer to those compound classes that are currently encountered in environmental compartments and have impacted the wildlife and trophic chain, yet they are still unregulated.<sup>5,6</sup> The European Commission fully aware of this fact has already launched the first and second “Watch List”<sup>7,8</sup> that refer to those substances or family classes for which monitoring data ought to be gathered for the purpose of human risk exposure and assessment.

Appropriate risk exposure of those compounds is associated to the so-called exposomic studies. Exposomics refers to the combination of exposures to a number of chemical and physical stressors along with human genetics that might account for chronic human diseases.<sup>9</sup> The main challenge of the exposomics workflow is to explore and identify actual human exposures via epidemiological studies of an individual in a holistic format, including those related to the environment, diet, and endogenous processes.<sup>10</sup> To tackle this challenge, environmental metabolomics has become an emerging discipline in the field of exposomics, and is based on the use of model animals (e.g., earthworms) to identify a number of endogenous metabolites as potential biomarkers of contaminant exposure.<sup>11</sup>

It should be however noted that the REACH regulation is currently promoting alternative methods to *in-vivo* assays for the hazard assessment of substances in order to reduce the number of tests on animals.<sup>12</sup> *In-vitro* assays seem to fulfil REACH demands, yet method development to get insight into potential toxicity effects on biota is not straightforward. In fact, a pivotal issue of *in-vitro* testing is to elucidate mechanisms at the molecular level for inferring permeability and distribution of contaminants in cell membranes within the broad concept of environmental bioavailability,<sup>13,14</sup> as defined by ISO 17402:2008.<sup>15</sup> In fact, bioavailability refers to the chemicals or fraction thereof that can interact with or pass across a biological membrane. To this end, biorelevant membrane surrogates of eukaryotic cells as a proxy of lipid bilayers are in *in-vitro* bioavailability tests called for. Lipid-based nanoparticles, also termed liposomes,<sup>16-18</sup> have been consolidated as mock cellular membranes for the *in-vitro* exploration of supramolecular interactions of chemical compounds with the phospholipids integrating biological membranes.<sup>19,20</sup> Because phosphatidylcholine (PC) is the most abundant phospholipid

in eukaryotic membrane cells *in-situ* synthesized large unilamellar vesicles/liposomes (LUV) from natural sources of PC containing both saturated and unsaturated chains has been herein selected as a model of biological membranes.

This work proposes for the first time a multidisciplinary *in-vitro* approach for environmental bioavailability studies based on the exploration of membrane permeability, and validated by four model compounds, representative of three classes of emerging contaminants<sup>1</sup>, namely diclofenac (DCF) as a model of anti-inflammatory drug that was included in the first EU Watch List, triclosan (TCS) as anti-microbial agent, and bisphenol A (BPA) as a plastic additive, and compared against a legacy insecticide, *viz.*, clorpyrifos (CPF), endorsed by the current EU Water Framework Directive.<sup>21</sup> The model analytes are characterized by varying physicochemical properties, including acid-base behavior ( $pK_a$  values), octanol-water partition ( $\log P_{\text{oct/water}}$ ) values, van der Waals volumes and dipole moments, the last two calculated using Density Functional Theory calculations and also EC50/LC50 values for distinct trophic levels that are estimated on the basis of impairment/mortality of zebrafish (*Danio rerio*) embryos, immobility/mortality of *Daphnia sp.*, and luminescence inhibition of *Vibrio fischeri* (see Table 1).

Both empirical and theoretical *in-silico* studies have been selected to mechanistically infer molecular interactions of the above compounds and potential bioavailability and bioaccumulation via passive diffusion. Two fluorescent membrane probes bearing naphthalene moieties (*viz.*, 6-propionyl-2-dimethylaminonaphthalene (prodan) and 6-dodecanoyl-2-dimethylaminonaphthalene (laurdan) have been chosen to ascertain low-resolution changes in bilayer organization by generalized polarization (GP) or fluorescence anisotropic ( $r_{ss}$ ) measurements that serve to indicate alterations in lipid ordering and liposome fluidity, respectively.<sup>22-25</sup> The low-resolution fluorescence results have been complemented by high-resolution NMR spectroscopy. The use of Diffusion-Ordered NMR Spectroscopy (DOSY) experiments allow elucidating whether or not the contaminants are bound to the liposomes. In addition, 2D  $^1\text{H}, ^1\text{H}$ -ROESY (Rotating frame Overhauser Effect Spectroscopy) and  $^1\text{H}, ^1\text{H}$ -NOESY (Nuclear Overhauser Effect Spectroscopy) experiments,<sup>26</sup> together with potential  $^1\text{H}$

chemical shift perturbations in the course of vesicle titration assays would provide relevant insights on the favorable interaction/s occurring at atomic resolution. This empirical approach is expected to elucidate the molecular interaction and the extent of binding of targets to biomembrane surrogates, and thus enable identification of potentially hazardous chemical compounds. Empirical data are to be supplemented by theoretical calculations based on Molecular Dynamics (MD) simulations using a realistic model of lipid bilayer that might offer invaluable insight at the molecular level into the penetration of each contaminant across the hydrophilic and hydrophobic regions of phospholipids.<sup>27,28</sup>

## MATERIALS AND METHODS

Detailed information and description of (i) reagents and target compounds, (ii) synthesis of liposomes, (iii) assignment of  $^1\text{H}$  NMR signals from liposomes, (iv) permeability of contaminants across liposomes elucidated by  $^1\text{H}$  NMR, and (v) theoretical molecular dynamic studies, is available as supporting information (SI).

In brief, the synthesis of the large unilamellar vesicles (LUV) made of phosphatidylcholine (PC) was performed from multilamellar vesicles (see SI) by extrusion through a 100 nm pore size polycarbonate filter. The potential alteration of phospholipid packing and ordering at distinct regions of LUVs in the presence of bioavailable contaminants was investigated by fluorescent membrane probes (laurdan and prodan) at 37°C. Contaminant-dependent alteration of the fluidity of the membrane was also investigated by laurdan anisotropic measurements (see below). Preliminary control experiments were undertaken to demonstrate that the structural integrity of the liposomes was not jeopardized with the maximum percentage of methanol from the standards of the target compounds added to the liposomal solution ( $\leq 0.4\%$  methanol). The NMR assignment of the signals of PC liposomes was carried out using 1D- $^1\text{H}$ , 2D- $^1\text{H}$ ,  $^1\text{H}$ -NOESY and 2D- $^1\text{H}$ ,  $^1\text{H}$ -ROESY experiments. NOESY and ROESY are NMR experiments that allow establishing correlations between different  $^1\text{H}$  that are physically close to each other regardless they are bonded or not. Typically,  $^1\text{H}$ ,  $^1\text{H}$ -ROESY experiments are used for molecules

of relatively low molecular weight (<1k Da) because their NOE (Nuclear Overhauser Effect) effects are too weak to be detectable. In our work, 1D-<sup>1</sup>H, 2D-<sup>1</sup>H,<sup>1</sup>H-NOESY and 2D-<sup>1</sup>H,<sup>1</sup>H-ROESY assays were also used to study the supramolecular interactions between the different contaminants and the PC liposomes, which were performed by titration experiments. 1D-<sup>1</sup>H, 2D-<sup>1</sup>H,<sup>1</sup>H-NOESY and 2D-<sup>1</sup>H,<sup>1</sup>H-ROESY experiments were acquired by using a water suppression pulse sequence. The potential formation of a supramolecular complex between PC liposomes and the various contaminants was assessed by using diffusion-ordered NMR spectroscopy (DOSY), which is able to provide insights on the diffusion coefficients of the different molecules in solution, and thus on the hydrodynamic radius of the molecule. Finally, the molecular dynamics (MD) simulations were performed by using the united-atom approximation and conducted on a fully hydrated palmitoyl-linoleylphosphatidylcholine (C18:2/C16:0, PLPC) topology that was arranged in a bilayer of 64 lipid molecules per leaflet.

#### **Permeation of contaminants across lipid bilayers as identified by liposome-based fluorescence assays**

In this section, experimental details of fluorescence-based permeation tests of contaminants using membrane probes and liposomes are described. First, a stock solution of liposomes (12.4 mM PC, see SI) was prepared and diluted to 100  $\mu$ M in PBS and stored in a brown glass vial. Then, a metered volume of laurdan or prodan in DMSO was added to the liposomal suspension at a final concentration of 1  $\mu$ M and kept in darkness and at room temperature for at least 75 min for laurdan, and 10 min for prodan to obtain constant fluorescent values that indicate steady-state conditions for the fluorescent probe between the liposomal membrane and the external aqueous medium. An additional incubation time of 15 min was used for the contaminants (final concentrations of 50, 100, 150 and 200  $\mu$ M) to reach the liposomal partition equilibrium.

Steady-state fluorescence assays were performed using a Varian Cary Eclipse fluorescence spectrometer (Agilent technologies, Mulgrave, Victoria). The samples were incubated at 37 °C

in the peltier multicell holder for 5 min prior to measurement. Fluorescence emission spectra were recorded from 400 to 600 nm by setting the excitation wavelength to 360 nm, and the photomultiplier detector voltage to 550 V with slit widths of 10 nm. The modification of lipid packing and ordering upon penetration of the organic contaminants into the bilayer was measured by the Generalized Polarization (GP) equation (Eq. 1):

$$GP = \frac{I_B - I_R}{I_B + I_R} \quad (\text{Eq. 1})$$

where  $I_B$  and  $I_R$  stand for the fluorescence emission intensities at 440 nm and 490 nm, respectively, corresponding to the maximum emission of the membrane probes in nonpolar media and aqueous solutions, respectively. Theoretically GP values range from -1 to +1. Negative values refer to a liquid-crystalline phase, and the gel phase, which is characterized by a more ordered and dehydrated membrane, provides positive values of GP.

Contaminant-dependent alteration of the fluidity of the membrane by bioavailable species was investigated by laurdan anisotropy detection using the fluorimeter polarizers. Samples were prepared as described previously. Steady state anisotropy ( $r_{ss}$ ) was carried out in L-format at excitation and emission wavelengths of 350 nm and 440 nm, respectively. The photomultiplier voltage and slits were fixed to 600V and 10 nm, respectively. The  $r_{ss}$  values were obtained from the manufacturer's software using the following equation (Eq. 2):

$$r_{ss} = \frac{I_{VV} - GI_{VH}}{I_{VV} + 2GI_{VH}} \quad (\text{Eq.2})$$

where  $I_{VV}$  and  $I_{VH}$  stand for the fluorescence emission intensities at the vertical and the horizontal emission polarizers, respectively, with the excitation light in vertical mode. The  $G$  factor provided by the fluorimeter is used as a monochromator correction.

## RESULTS AND DISCUSSION

### Decoding the membranotropic effects of environmental contaminants using membrane fluorescent probes



Membranotropic effects are herein used for evaluation of the potential contaminant bioavailability. In the case of TCS, a strong hypsochromic Stock (blue) shift of the maximum emission wavelength of laurdan (Figure S1) is observed by increasing TCS concentrations, thus suggesting a perturbation of the probe microenvironment polarity as a result of TCS bioavailability. This might occur as a consequence of a TCS-triggered membrane dehydration process occurring at the probe surrounding, which is located at the hydrophilic-hydrophobic interface of the lipid bilayer.<sup>29</sup> This effect was also observed when the LUVs were titrated with BPA, DCF or CPF, but to a much lesser extent (Figures S2-S4). In addition, the titration of LUVs with BPA afforded two clearly distinguishable fluorescence bands (Figure S2). The addition of BPA most likely drives laurdan to exhibit two different but notably populated environments and implies that only a part of the hydrophilic-hydrophobic interface of the liposome is hydrated. However, fluorescent phenomena other than solvent dipolar relaxation might also occur.<sup>30</sup>

The increase of laurdan's Generalized Polarization (GP) values calculated by Eq. 1 is indicative of the packed structure of the lipid bilayer in the presence of the contaminants as well as of the membrane dehydration level. Figure 1A (illustrating the addition of contaminant at 50  $\mu\text{M}$ ) revealed that a maximum GP increase -as compared to laurdan alone- occurs for BPA, followed by TCS, CPF and DCF (see Figures S1-S4 for visualization of spectral shifts and SI for the equation of GP). One-way ANOVA could not be applied in our case because of the identification of heteroscedastic data for some compounds, and thus non-parametric methods should be used instead. In fact, the *t*-tests of comparison of means revealed the existence of significant differences at  $\alpha=0.05$  between the GP value of the probe alone and those obtained in the presence of individual compounds. However, DCF has the lesser permeability by passive diffusion into the LUVs. This is in good agreement with previous results by Suwalsky *et al.*<sup>31</sup> who reported slight variations of Laurdan GP up to 2 mM DCF. In addition, the trends of GP values are highly concentration dependent (Figure 1B), because e.g. TCS and CPF induce an enhanced lipid ordering and compact structural assembly at concentrations above 100  $\mu\text{M}$  as identified by the sharp increase in GP.

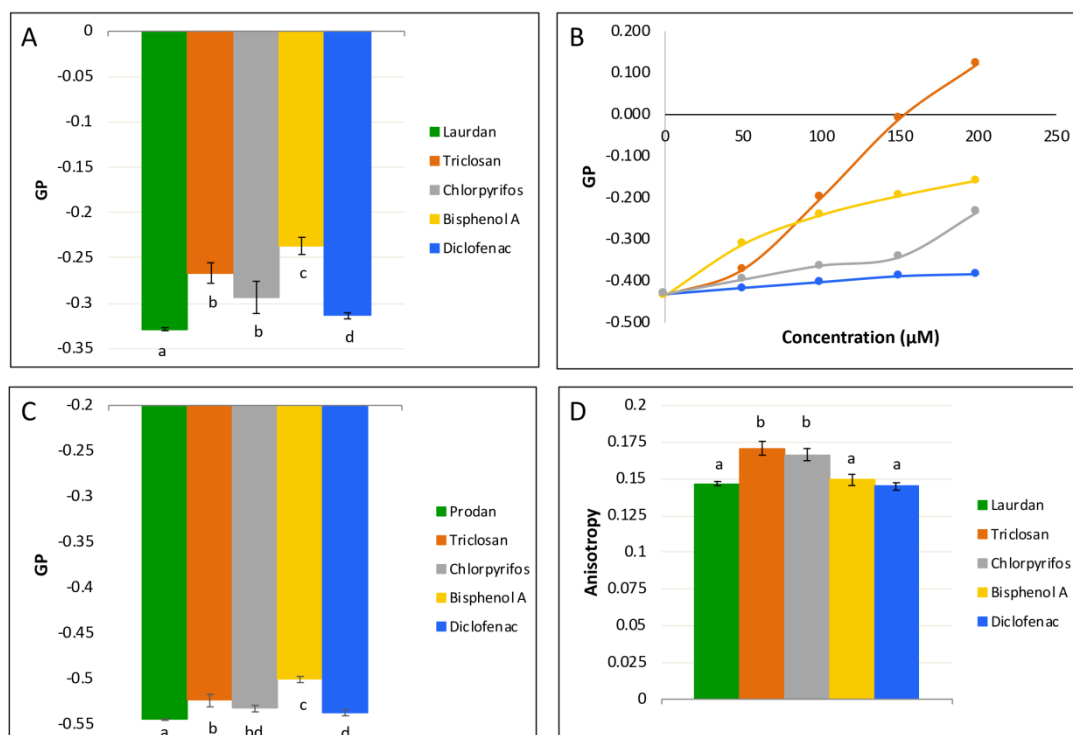


Figure 1. Fluorescence studies of soy PC LUVs at 37°C using laurdan and prodan as membrane probes. (A) Laurdan's GP values obtained with PC LUVs in the presence of various organic contaminants at the concentration level of 50  $\mu\text{M}$ . (B) Laurdan's GP values obtained for PC LUVs at different concentration levels of each studied contaminant (50, 100, 150 and 200  $\mu\text{M}$ ). Data corresponding to TCS is shown in *orange*, that corresponding to CPF is shown in *grey*, that corresponding to BPA is shown in *yellow* and data for DCF is shown in *blue*. (C) Prodan's GP values obtained with PC LUVs in the presence of various organic contaminants at a concentration level of 50  $\mu\text{M}$  (D) Fluorescence anisotropy measurements for laurdan-embedded PC liposomes with various individual contaminants at the concentration level of 50  $\mu\text{M}$ . Statistical tests were based on *t*-tests of comparison of means at a significance level ( $\alpha$ ) of 0.05.

The GP values obtained for prodan as a probe revealed that the four contaminants follow the same trend than that observed for laurdan (Figure 1C), with statistically significant GP differences in all cases against prodan alone. Again, the influence of bisphenol A on GP was stronger than that of the other pollutants. However, a smaller variation of average prodan GP data is measured for all of the targets when compared to the probe alone. This observation can be attributed to the ability of prodan to interact with both the external water molecules and the polar head of the LUVs<sup>32</sup> as corroborated by the more negative GP values compared to those of laurdan. Consequently, the polarity of the medium around prodan is much less affected by the organic contaminants. In fact, DFT calculations indicate that the binding energy of prodan at the polar head of the phospholipid is akin to that at the glycerol region,<sup>32</sup> yet its intercalation into the

lipid molecules would require the separation of the acyl chains. Our conclusion is that the shallow prodan might not serve as a good indicator of the molecular interaction of contaminants with PC lipid bilayers in order to investigate compound bioavailability, but prodan could be useful in liposomal media with phospholipid composition other than > 98% PC.

Fluorescence spectroscopy was also used to explore anisotropic effects ( $r_{ss}$ , Eq. 2). Laurdan anisotropy was only affected, in a statistically significant manner ( $\alpha=0.05$ ), by TCS and CPF (Figure 1D). The increase of the  $r_{ss}$  values from ~0.15 to ~0.17 suggests that the liposomal microviscosity is enhanced by the above contaminants,<sup>32</sup> whereas the fluidity of the phospholipid bilayer remained unaltered with the addition of either BPA or DCF to the LUVs. These anisotropic data disagree with the conclusions derived from laurdan's GP data for BPA. This might evidence the existence of an indirect relationship between the laurdan's spectral changes and the effect of BPA at the glycerol backbone level where laurdan is located.<sup>32</sup> Consequently, the permeability of BPA throughout the lipid bilayer, and thus its bioavailability, cannot be unequivocally identified from the analysis of the fluorescent spectral shifts of laurdan. It should be also noted that laurdan's anisotropy serves as a better *in-vitro* indicator for discrimination of the degree of penetration of xenobiotics across membranes as compared to GP measurements because statistically different anisotropy values against laurdan alone are obtained only for two out of the four contaminants investigated.

To shed light on the discrepancies between the GP and the anisotropic data for BPA as a target contaminant, the potential effect of BPA on the fluorescence emission spectrum of laurdan embedded in the vesicles was explored. Hence, fluorescence quenching effects were analyzed by the Stern-Volmer equation.<sup>33</sup> Our findings (Figure S5) revealed that BPA and DCF do induce a negligible quenching effect of the fluorescence intensity of laurdan ( $K_{SV} < 0.025 \mu\text{M}$ ), as opposed to TCS and CPF that seem to induce a subtle quenching effect, which would involve both dynamic and static processes as suggested by their non-linear Stern-Volmer plots. Consequently, the disagreement between the anisotropic and GP data for BPA is most likely a consequence of molecular effects other than fluorescent quenching.

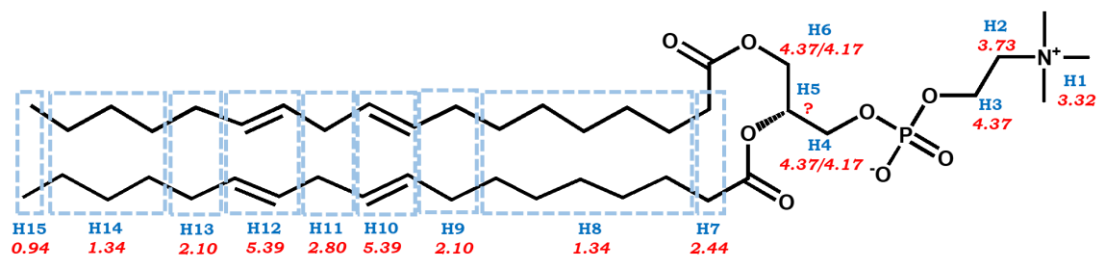


**Figure 2.** Chemical structure of 1,2-dilinoleoyl-*sn*-glycero-3-phosphocholine (DLPC, PC-18:2). C-H groups that displayed indistinguishable chemical shifts have been grouped in square dashed blue boxes. In addition, C-H moieties have been arbitrarily labelled as H<sub>n</sub> (*blue*), and their <sup>1</sup>H chemical shifts are given in ppm (*red*).

### <sup>1</sup>H NMR mapping of the PC liposome-binding regions upon interaction with contaminants

Our results clearly demonstrate that the fluorescent data provided by membrane probes should be analyzed thoroughly because the specific chemical nature of the contaminant, as well as the direct or indirect effects onto the lipid assembly and/or on the fluorescent probe might lead to misleading bioavailability interpretations. Therefore, fluorescence data necessarily need to be supplemented by high resolution experimental techniques. Consequently, NMR spectroscopy has been employed to get insight at the atomic level on the specific architecture of the interactions occurring between soy PC LUVs and each contaminant to shed light upon the bioavailability of the target species (see SI for experimental methodology).

The <sup>1</sup>H-NMR assignment of 1,2-dilinoleoyl-*sn*-glycero-3-phosphocholine (PC 18:2, DLPC) was obtained at pD 7.4 and 37°C using standard 1D and 2D NMR experiments. Despite the significant signal broadening as a result of the low molecular tumbling of the LUVs, the <sup>1</sup>H-NMR assignment could be accomplished for all of the protons, except for H5 (Figure 2), which likely appears under the suppressed water signal.

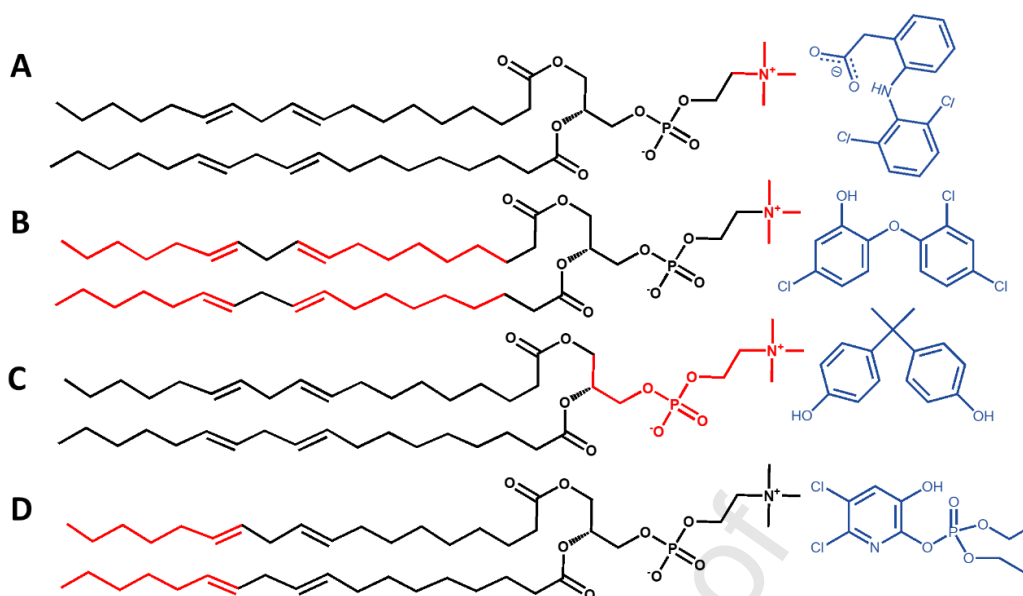
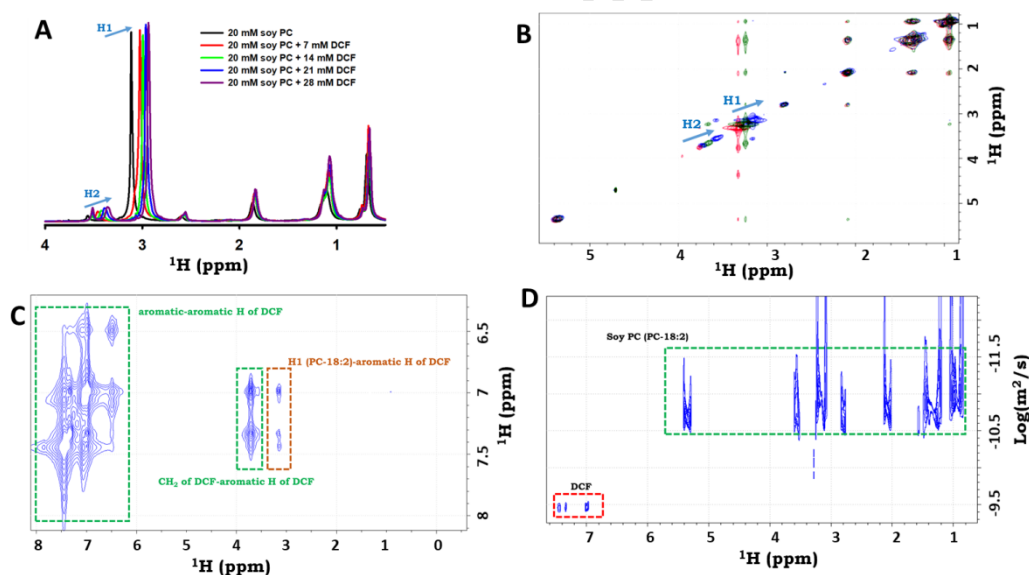
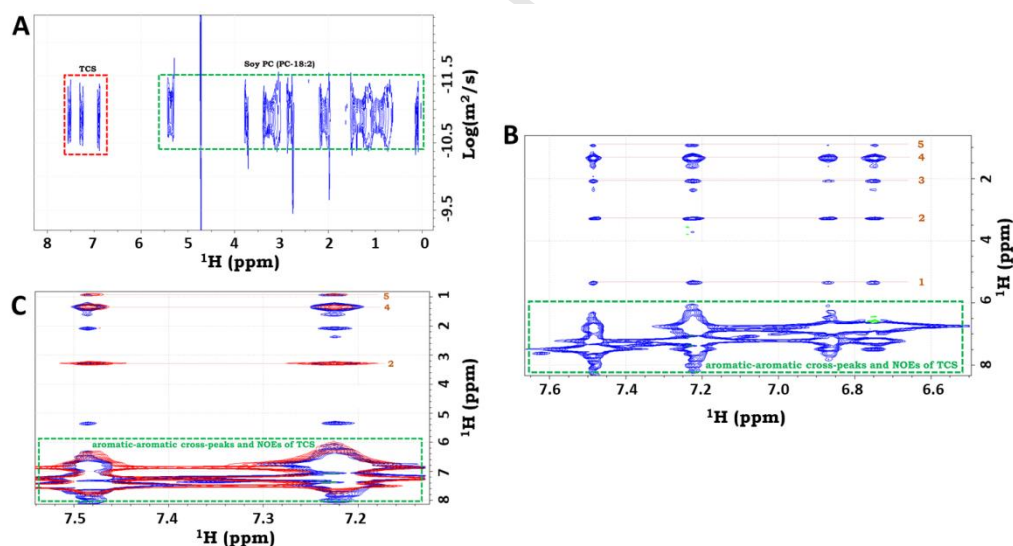


**Figure 3.** Chemical structures of PC-18:2 (A-D), DCF (A), TCS (B), BPA (C) and CPF (D). The chemical structure of the different contaminants (ligands) are shown in blue, whereas the C-H groups of PC-18:2 displaying chemical shift perturbations and/or intermolecular NOE with each contaminant at pD 7.4 (in 20mM phosphate buffer) are colored in red.



according to the numbering given in Figure 2. (B) Overlapping of the  $^1\text{H}$ ,  $^1\text{H}$ -NOESY spectra of soy PC LUVs alone (red) and with DCF at 7mM (green) and 28mM (blue). The cross-peaks displaying a higher chemical shift perturbation as a result of the DCF addition, are labeled according to the numbering given in Figure 2. (C) Aromatic region of the  $^1\text{H}$ - $^1\text{H}$  NOESY spectrum of a mixture containing soy PC LUVs (20mM) and DCF (28mM). The aromatic-aromatic cross-peaks of DCF, as well as their intramolecular NOEs are squared in a green dashed box. The intermolecular NOEs between the aromatic protons of DCF and the H1 protons of PC-18:2 are squared in a brown dashed box. (D) 2D-DOSY spectrum of a mixture containing soy PC vesicles (20mM) and DCF (28mM). The  $^1\text{H}$  signals of the soy PC LUVs have been squared in a dashed green box, whereas those corresponding to DCF has been squared in a dashed red box.

The NMR assignment allowed us to map the interaction region between the PC 18:2 (DLPC) molecules that constitute the LUVs and each contaminant (Figure 3). The addition of DCF only induced significant chemical shift perturbation on the signals corresponding to H1 and H2 at pD 7.4 (Figures 4A, B), which indicates that DCF mainly interacts with the outer polar moieties of PC (Figure 3A). This might occur through an electrostatically driven process as a result of the binding between the  $-\text{CH}_2-\text{N}(\text{CH}_3)^+$  moiety of the PC 18:2 and the carboxylate moiety of DCF. However, the appearance of NOEs between the aromatic protons of DCF and the H1 protons of PC-18:2 (Figure 4C) suggested that a cation- $\pi$  interaction is occurring between the choline group and the DCF that would position the aromatic rings perpendicular to the LUV surface. On the other hand, the DOSY spectra revealed that the relative diffusion coefficient ( $D$ ) of DCF (Figure 4D) was notably different to that displayed by the soy PC LUVs, which indicates that DCF in solution does not interact with the liposomes to a large extent. Consequently, our results demonstrated that the binding between DCF and soy PC LUVs only occurs on the vesicle surface, although this process seems not to be thermodynamically favored.



spectrum of a mixture containing soy PC LUVs (20mM) and TCS (17mM) prepared in 20mM  $\text{D}_2\text{O}$  phosphate buffer at pD 7.4. The  $^1\text{H}$ - $^1\text{H}$  cross-peaks of TCS and its intramolecular NOEs are squared in a dashed green box. The intermolecular NOEs detected between the aromatic protons of TCS and the protons of the soy PC LUVs are labelled as follows: i) the H10 and/or H12 of PC-18:2 (1); ii) the H1 of PC-18:2 (2); iii) the H13 and/or H9 of PC-18:2 (3); iv) the H14 and/or H8 of PC-18:2 (4); and v) the H15 of PC-18:2 (5). The numbering of each proton is given in Figure 2. (C) Overlapping of the  $^1\text{H}$ ,  $^1\text{H}$ -NOESY spectra of mixtures containing soy PC LUVs (20mM) and TCS (17mM) prepared at pD 7.4 (blue) and at

pD 4.7 (*red*). The  $^1\text{H}$ - $^1\text{H}$  cross-peaks of TCS and its intramolecular NOEs are squared in a dashed green box. In addition, the intermolecular NOEs detected between the aromatic protons of TCS and the protons of the soy PC LUVs are labelled as described in the figure caption of panel (B).

With respect to TCS, its low solubility in water ( $\sim 35 \mu\text{M}$  at  $20^\circ\text{C}$ ) might jeopardize the NMR interaction studies. However, the solubility of TCS was notably increased with the addition of vesicles. For instance, TCS at 17 mM concentration was completely dissolved in a 20mM liposome-containing solution. The DOSY spectrum of the TCS-liposome mixture suggests that TCS is embedded in the LUVs, because both TCS and LUVs displayed the same  $D$  value (Figure 5A). This observation was additionally confirmed by the  $^1\text{H}$ , $^1\text{H}$ -NOESY spectrum, which clearly showed intermolecular NOEs between the aromatic protons of TCS and the H10 and/or H12; H1; H13 and/or H9; H14 and/or H8; and H15 of PC-18:2 (Figure 5B). These results demonstrated that TCS is able to interact with the polar head groups of the PC vesicle surface, but most importantly with the hydrophobic core of the LUVs. To assess whether the surface binding was due to the interaction between the cationic choline of PC 18:2 and the phenolate form of TCS (its  $\text{pK}_a$  is  $\sim 7.9$  and therefore,  $\sim 33\%$  of TCS is under the phenolate form at pD 7.4), the  $^1\text{H}$ , $^1\text{H}$ -NOESY spectrum was also recorded at pD 4.7, for which the percentage of negatively charged TCS is negligible. Strong intermolecular NOEs involving H1 of PC 18:2 (Figure 5C) were still observed. This finding suggests that the LUV surface likely binds TCS through a cation- $\pi$  interaction.<sup>34</sup> The lack of NOEs involving the H10 and H12 groups indicates that TCS at this pD likely penetrates deeply across the fatty acid region of the LUV and it is tightly bound to the inner hydrophobic tail of the bilayer (Figure 3B).

As for BPA, the NMR DOSY spectrum revealed that this emerging contaminant is able to interact with soy PC LUVs at pD 7.4 (Figure 6A). The NMR titration of LUVs with BPA evidenced that NMR readouts corresponding to H1, H2 and H3 of PC 18:2 were the only ones that modified their chemical shifts upon adding BPA (Figure 6B). Consequently, BPA preferentially interacts with and accumulates at the polar head region of PC 18:2 (Figure 3C), and thus only minute amounts might penetrate into the hydrophobic core of the vesicle. This is likely occurring because both phenol groups of BPA are tweezing the choline moiety through



the anchoring of the hydroxyl group to the polar head group of PC. The unambiguous intermolecular ROE signals between the H1 of PC 18:2 and the *ortho*-position protons of BPA but the inexistence of signals with those at *meta*- position nor with the methyl groups (Figure 6C) supported the interaction mechanism hypothesized. Accordingly, our results demonstrate that the supramolecular interaction of PC liposomes with BPA exists but their binding is limited to the vesicle surface. This fully agrees with the NMR data reported by Malekar *et al.*<sup>35</sup>

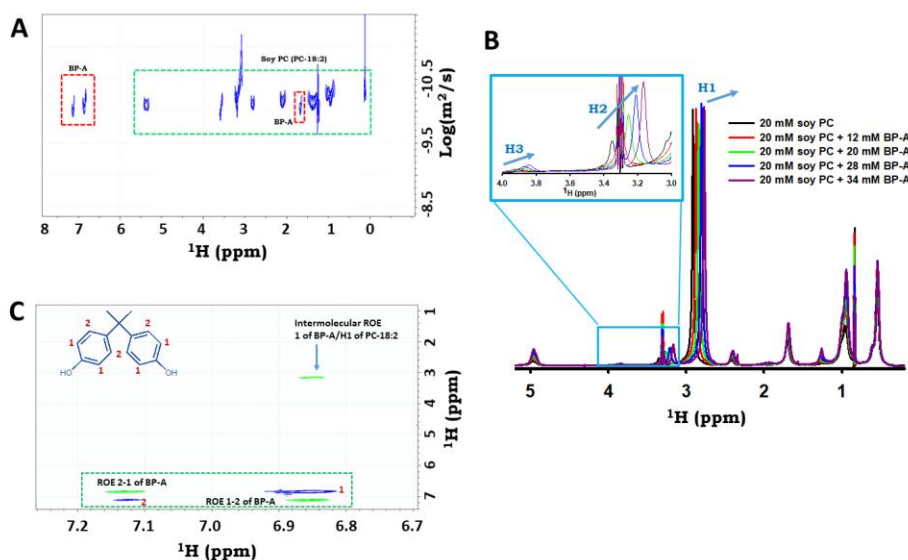


**Fig**  
spe  
buf  
box

the aliphatic region of the  $^1\text{H}$ -NMR spectra of soy PC with increasing concentrations of BPA. The signals displaying a higher chemical shift perturbation as a result of the BPA addition are labeled according to the numbering given in Figure 2. The insert shows a zoom of the region between 3 and 4 ppm. (C)  $^1\text{H}$ ,  $^1\text{H}$ -ROESY spectrum of a mixture containing soy PC LUVs (20 mM) and BPA (34 mM) in 20 mM  $\text{D}_2\text{O}$  phosphate buffer at pH 7.4. The blue signals correspond to the aromatic cross-peaks of BPA, whereas the green signals correspond to the intramolecular BPA ROEs (squared in a green box), and to the intermolecular BPA/PC-18:2 ROE observed between the H1 protons of PC-18:2 and the protons at the *ortho* position of BPA.

Elucidation of the degree of penetration of CPF across the biomembrane surrogate was also investigated. The addition of CPF to a solution containing PC LUVs afforded supramolecular interactions, as both the contaminant and LUVs displayed similar  $D$  values (Figure 7A). In fact, CPF induced chemical shift perturbations on the  $^1\text{H}$ -NMR signals that are characteristic of the hydrophobic core of the LUV (i.e. H12, H13, H14 and H15) (Figure 7B). The binding between CPF and the hydrocarbonated tail of the PC 18:2 was additionally confirmed by the



identification of intermolecular NOEs between the H15 and H14 moieties of the PC 18:2 and the aromatic proton of CPF (Figure 7C), thus confirming that CPF is capable of entering into the lipid bilayer and remain predominantly at the inner hydrophobic region. Moreover, the  $^1\text{H}, ^1\text{H}$ -NOESY spectrum revealed that intramolecular NOEs between the aromatic proton of CPF and methyl moieties do occur. This observation suggests that CPF inside the PC liposomes might adopt a tripod-like conformation, where the aromatic ring and the two methyl groups would form the hypothetical tripod base. Consequently, our data demonstrate that CPF strongly interacts with soy PC liposomes as a highly bioavailable organic compound (Figure 3D). Experimental results obtained for the target compounds by laurdan GP and anisotropic fluorescence measurements and  $^1\text{H}$ -NMR chemical shift perturbations at the hydrophobic tail of the bilayer were compared with IC50/LC50 literature data of three ecotoxicological assays (see Table 1). A good correlation was found between those compounds that cause severe membranotropic effects onto liposomes and toxicity data. Indeed, the degree of penetration of a given contaminant across the lipid bilayer seems to serve as an invaluable indicator of bioavailability and potential toxicity effects; the greater the interaction with the fatty acyl chains of the PC, as is the case with CPF and TCS, the lower are the IC50/LC50 values.

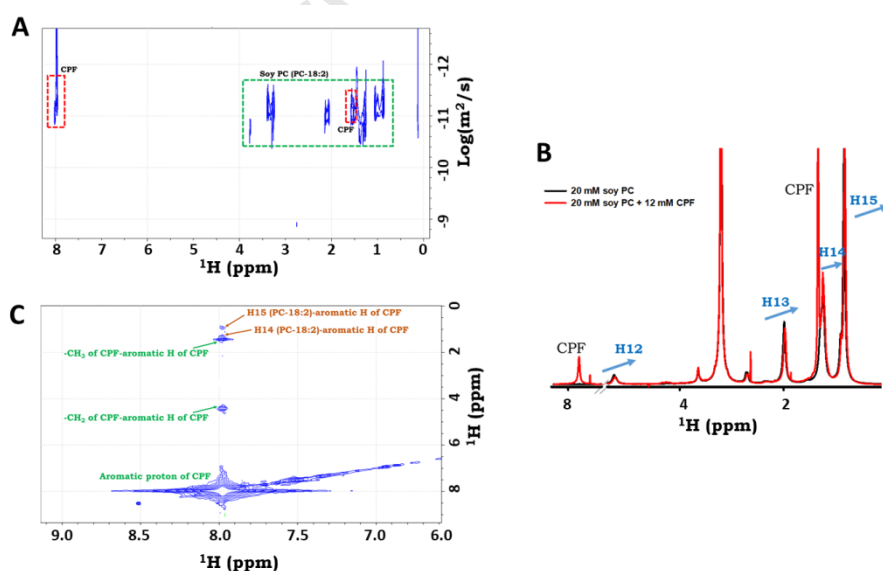


**Figure 3.**  $^1\text{H}$ -NMR spectra of soy PC LUVs without and with CPF at the 12mM level. The signals displaying

a higher chemical shift perturbation as a result of the CPF addition are labeled according to the numbering given in Figure 2. (C)  $^1\text{H}, ^1\text{H}$ -NOESY spectrum of a mixture containing soy PC vesicles (20mM) and CPF (12mM) in 20mM  $\text{D}_2\text{O}$  phosphate buffer at pD 7.4. Intramolecular NOEs detected for CPF are labelled in green. Intermolecular NOEs observed between CPF and PC-18:2 are labelled in brown.

### Molecular dynamics of the different contaminants across the lipid bilayer

The binding process between individual contaminants and the soy PC LUVs can be understood better if the elucidation of the molecular interaction regions is supplemented with dynamical information on the most probable locations of the bilayer in which the contaminant is situated after penetrating into the LUVs. In this context, molecular dynamic (MD) simulations have become a powerful tool. Because soy PC LUVs consists of both saturated and unsaturated fatty acid chains, a computational model (see SI for further details) was built using a fully hydrated palmitoyl-linoleylphosphatidylcholine C18:2/C16:0 (PLPC) phospholipid. Initially, all the studied compounds were introduced into the water layer that solvates the biomembrane and then, the entire system was allowed to equilibrate.

The average area per lipid ( $A_{\text{PLPC}}$ ) is a useful parameter to describe the packing of the lipid molecules within the bilayer, and to evaluate the stability of the bilayer during the MD simulations. The  $A_{\text{PLPC}}$  values and the bilayer thickness ( $h$ ) for PLPC are similar to those previously reported by Wong-ekkabut *et al.*<sup>36</sup> In addition, the  $A_{\text{PLPC}}$  and  $h$  values were highly homogeneous across the different models (probes and contaminants), and were in good agreement with values reported for similar membranes (*e.g.*, areas spanning from 0.62 to 0.68  $\text{nm}^2$  for DPPC)<sup>37</sup> (see Table 2). The lateral diffusion coefficients ( $D_{\text{lat}}$ ) of the lipid bilayer for every contaminant were obtained by the Einstein relation, using the slope of the average mean square displacement after equilibration.<sup>38</sup> The computed values agreed well with experimental neutron scattering diffusion coefficients ( $(5-100)\times 10^{-8} \text{ cm}^2/\text{s}$ ),<sup>39,40</sup> which serves as a validation of the MD methodology herein proposed.

The evaluation of the data in Table 2 gives us invaluable information of the most favorable location of the contaminants within the bilayer, thus shedding light onto the potential bioavailability and bioaccumulation of the target species. For example, the  $D_{\text{lat}}$  value of PLPC in the presence of DCF is larger than that observed for laurdan or prodan. This finding suggests

that DCF interacts merely with the phospholipid head groups of the lipid bilayer, mostly with the choline moiety, which agrees with our fluorescence and NMR data and previous data in the literature.<sup>41</sup> In contrast, the  $D_{lat}$  value of CPF is smaller than those of the probes, thus indicating that CPF increases the packing of the lipids, likely due to the non-covalent van der Waals interactions that necessarily should be stronger than those between lipids. The hindrance of the lateral diffusion of PLPC with the addition of CPF as indicator of bioavailability and bioaccumulation is in excellent agreement with both laurdan's GP and anisotropy data that indicate lipid ordering and rigidity, respectively, and also with NMR measurements for which NOEs are identified at the hydrophobic tail of the fatty acyl chain.

Further insight into the ease of penetration of the contaminants across the bilayer can be obtained throughout the mass density profile. Figure 8 illustrates the most likely position of the xenobiotic and probe with respect to the center of the bilayer (apolar–apolar interface) in the time course of the MD simulation. The naphthalene group of laurdan is predominately located at the head-tail interface of the PC bilayer (Figure 8), according with its expected behavior in previous DOPC bilayers,<sup>42,43</sup> and prodan is freely movable, yet mainly positioned below the glycerol region, in accordance with previous MD simulations on a DLPC bilayer.<sup>44</sup> Neutral and anionic charge states of TCS were simulated to understand the effect of the protonation on the degree of penetration. The anionic TCS mostly remains interacting with the polar head group, whereas the neutral TCS is inserted into the bilayer, which qualitatively agrees with our NMR data. MD simulations additionally revealed that BPA akin to neutral TCS is mainly located at the hydrophilic-hydrophobic interface of the PLPC, which is in good agreement with previous theoretical studies using DPPC bilayers.<sup>45</sup> Remarkably, TCS and BPA showed equal behavior across the PC lipid bilayer, notwithstanding the dissimilar log P values. However, the dipole moments and the van der Waals volumes for both molecules (see Table 1) are on a par, and thus the two molecular features seem to work as good indicators to elucidate compound permeability across lipid bilayers. On the other hand, CPF rapidly penetrates into the bilayer interface and, once located there, it is free to move through the two leaflets of the membrane. According to the NMR and MD data, the most likely location of CPF is at the hydrocarbon tails of lipids. Thus,

CPF is expected to be highly bioavailable/bioaccumulable and pose toxic effects to biota. Indeed, CPF is, out of the four contaminants, the one having the lowest IC50 and LC50 data for *Vibrio fischeri*, *Daphnia sp.* and *Danio rerio* (see Table 1). In contrast, DCF is mostly displaced on the membrane-water interface, and thus is less prone to cross the lipid membrane, as already suggested by the NMR and molecular fluorescence data. Data presented in Fig. 8 serve to estimate the absolute bioavailability values for every individual species on the basis of the MD timeframe that a compound is interacting with the alkylated chains of the PC. The MD-based absolute bioavailability values under passive diffusion were estimated as < 0.1%, 63%, 73% and 89% for DCF, BPA, TCS and CPF, respectively.

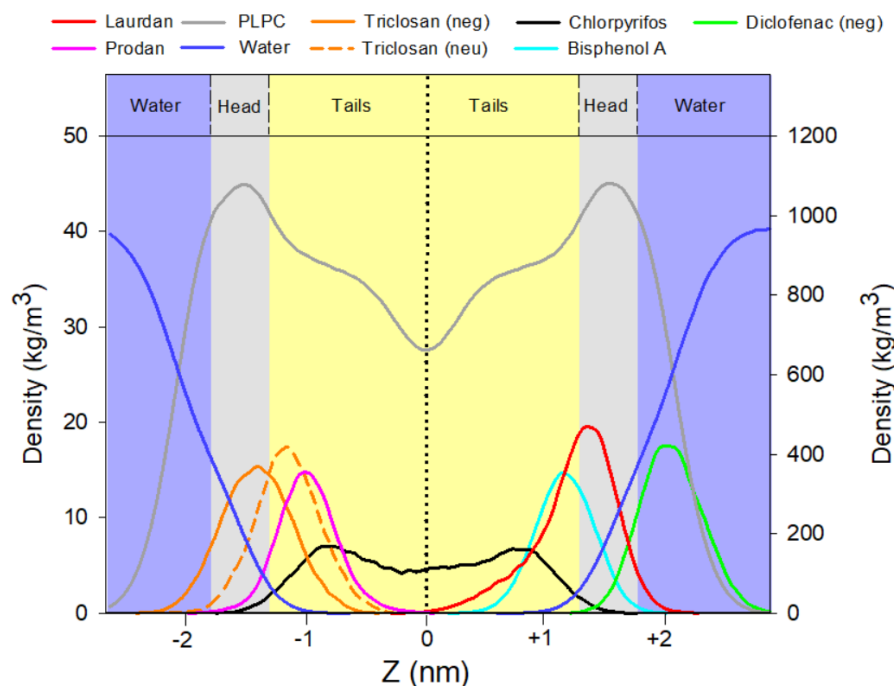


**Figure 8.** The average density profiles of water (blue line), PLPC lipid (gray line) in the right y-axis; triclosan-neg (negatively charged, orange solid line), triclosan-neu (uncharged, orange dashed line), Prodan (pink line), chlorpyrifos (black line), bisphenol-A (cyan line), laurdan (red line), diclofenac (green line) in the left y-axis as a function of the distance from the center of the lipid bilayer (Z).

## CONCLUSIONS

This study is aimed at filling the gap claimed by REACH and ISO 14702:2008 in developing *in-vitro* environmental bioavailability assays without animal models. Taking into account the fact

that the bioavailability concept involves the molecular interaction of species with cell membranes we have for the first time proposed a multidisciplinary empirical and theoretical approach using an elaborated model of phospholipid bilayer as a membrane surrogate. The theoretical simulations have corroborated that the lipid bilayer is a highly dynamic structure and that the contaminants might move freely within a wider or restricted region of the membrane and this fact helps predicting potential contaminant bioavailability and bioaccumulation. Our holistic approach has demonstrated that DCF is not prone to penetrate into the lipid bilayer at physiological pH to a large extent by passive diffusion, whereas CPF has the ability to do so as a highly bioavailable species and move rapidly across the hydrophobic region. While the results for DCF and CPF are somehow unambiguous, some uncertainties (at atomic level of resolution) are identified regarding the binding of TCS or BPA to the LUVs. In any case, all the results herein reported have pointed out that TCS binds to the cationic choline group of the LUVs but at the same time is able to easily penetrate deeply along the hydrophobic region. On the other hand, BPA seems to be preferentially interacting with the polar head group of the LUV. All these observations reinforce the idea that a multidimensional approach that is able to tackle the complexity of lipid bilayers mimicking eukaryotic cell membranes and explore membranotropic effects and contaminant distribution across membranes is needed.

Current work is underway to combine liposome-based bioavailability/bioaccumulation assays with physiologically-based extraction tests of organic contaminants in environmental solids for investigation of the uptake of bioaccessible species in body fluids (e.g., gastrointestinal compartment) across lipid bilayers in human exposomics studies.

### **Supporting information (SI)**

Detailed description of (i) materials, reagents and synthesis of liposomes, (ii) experimental methods based on the fluorescence detection of membrane probes embedded in liposomes and  $^1\text{H}$  NMR assignment of signals from liposomes, (iii) fluorescence emission spectra of laurdan embedded in liposomes after addition of individual contaminants, (iv)  $^1\text{H}$  NMR study of the supramolecular interaction between contaminants and liposomes, and (iv) molecular dynamic exploration of the mobility of contaminants across lipid bilayers.

**Acknowledgments**

Manuel Miró acknowledges financial support from the FEDER/Spanish Ministry of Science, and Innovation (MICINN)-Spanish State Research Agency (AEI) through projects CTM2017-84763-C3-3-R (MICINN/AEI/FEDER, EU) and CTM2017-90890-REDT (MICIU/AEI/FEDER, EU). Antonio Frontera extends his appreciation to AEI for the funding of project CTQ2017-85821-R (MICINN/AEI/FEDER, EU). Miquel Oliver thanks the Government of the Balearic Islands, Conselleria d'Educació, Cultura i Universitats, and the European Social Fund for PhD fellowship allocation (no. FPI/1681/2014).

Journal Pre-proof

## REFERENCES

- (1) Ebele, A. J.; Abou-Elwafa Abdallah, M.; Harrad, S. Pharmaceuticals and personal care products (PPCPs) in the freshwater aquatic environment. *Emerging Contaminants* **2017**, *3*, 1-16.
- (2) Fairbairn, D. J.; Arnold, W. A.; Barber, B. L.; Kaufenberg, E. F.; Koskinen, W. C.; Novak, P. J.; Rice, P. J.; Swackhamer, D. L. Contaminants of emerging concern: mass balance and comparison of wastewater effluent and upstream sources in a mixed-use watershed. *Environ. Sci. Technol.* **2016**, *50*, 36–45.
- (3) Reemtsma, T.; Berger, U.; Arp, H. P. H.; Gallard, H.; Knepper, T. P.; Neumann, M.; Quintana, J. B.; de Voogt, P. Mind the gap: persistent and mobile organic compounds water contaminants that slip through. *Environ. Sci. Technol.* **2016**, *50*, 10308–10315.
- (4) Lohmann, R.; Muir, D.; Zeng, E. Y.; Bao, L.-J.; Allan, I. J.; Arinaitwe, K.; Booij, K.; Helm, P.; Kaserzon, S.; Mueller, J. F.; Shibata, Y.; Smedes, F.; Tsapakis, M.; Wong C. S.; You, J. Aquatic Global Passive Sampling (AQUA-GAPS) revisited: first steps toward a network of networks for monitoring organic contaminants in the aquatic environment. *Environ. Sci. Technol.* **2017**, *51*, 1060–1067.
- (5) Schnoor, J. L. Re-emergence of emerging contaminants. *Environ. Sci. Technol.* **2014**, *48*, 11019–11020.
- (6) Richardson, S. D.; Ternes, T. A. Water analysis: Emerging contaminants and current issues. *Anal. Chem.* **2018**, *90*, 398–428.
- (7) Commission implementing decision (EU) 2015/495 of 20 March 2015 establishing a watch list of substances for Union-wide monitoring in the field of water policy pursuant to Directive 2008/105/EC of the European Parliament and of the Council, *Off. J. Eur.* **2015**, *L 78*, 40-42.
- (8) Commission Implementing Decision (EU) 2018/840 of 5 June 2018 establishing a watch list of substances for Union-wide monitoring in the field of water policy pursuant to Directive 2008/105/EC of the European Parliament and of the Council, *Off. J. Eur.* **2018**, *L 141*, 9-12.
- (9) Wild, C.P. Complementing the genome with an "exposome": The outstanding challenge of environmental exposure measurement in molecular epidemiology. *Cancer Epidemiol. Biomarkers Prev.* **2005**, *14*, 1847-1850.
- (10) Vrijheid, M. The exposome: A new paradigm to study the impact of environment on health. *Thorax* **2014**, *69*, 876-878.
- (11) Simpson, M.J.; McKelvie, J.R. Environmental metabolomics: new insights into earthworm ecotoxicity and contaminant bioavailability in soil. *Anal. Bioanal. Chem.* **2009**, *394*, 137–149.
- (12) Schoeters, G. The REACH perspective: Toward a new concept of toxicity testing. *J. Toxicol. Environ. Health B Crit. Rev.* **2010**, *13*, 232-241.

- (13) Ortega-Calvo, J. J.; Harmsen, J.; Parsons, J.R.; Semple, K.T.; Aitken, M.D.; Ajao, C.; Eadsforth, C.; Galay-Burgos, M.; Naidu, R.; Oliver, R.; Peijnenburg, W.J.G.M.; Römbke, J.; Streck, G.; Versonnen, B. From bioavailability science to regulation of organic chemicals. *Environ. Sci. Technol.* **2015**, *49*, 10255–10264.
- (14) Fedotov, P. S.; Kördel, W.; Miró, M.; Peijnenburg, W. J. G. M.; Wennrich, R.; Huang, P.-M. Extraction and fractionation methods for exposure assessment of trace metals, metalloids and hazardous organic compounds in terrestrial environments. *Crit. Rev. Environ. Sci. Technol.* **2012**, *42*, 1117-1171.
- (15) International Organization for Standardization. ISO 17402:2008. Soil quality: Requirements and guidance for the selection and application of methods for the assessment of bioavailability of contaminants in soil and soil materials. Geneva, Switzerland, 2008.
- (16) Janoff, A.S., Ed. *Liposomes: rational design*. Marcel Dekker: New York, 1999.
- (17) Lasic, D. D.; Barenholz, Y., Eds. *Handbook of nonmedical applications of liposomes*, vol. I-IV, CRC Press: Boca Raton, FL, 1996.
- (18) Li, J.; Wang, X.-L.; Zhang, T.; Wang, C.-L.; Huang, Z.-J.; Luo, X.; Deng, Y.-H. A review on phospholipids and their main applications in drug delivery systems. *Asian J. Pharm. Sci.* **2014**, *10*, 81–98.
- (19) Först, G.; Cwiklik, L.; Jurkiewicz, P.; Schubert, R.; Hof, M. Interactions of beta-blockers with model lipid membranes: Molecular view of the interaction of acebutolol, oxprenolol, and propranolol with phosphatidylcholine vesicles by time-dependent fluorescence shift and molecular dynamics simulations. *Eur. J. Pharm. Biopharm.* **2014**, *87*, 559–569.
- (20) Kovács, E.; Savopol, T.; Iordache, M. M.; Săplăcan, L.; Sobaru, I.; Istrate, C.; Mingeot-Leclercq, M. P.; Moisescu, M. G. Interaction of gentamicin polycation with model and cell membranes. *Bioelectrochemistry* **2012**, *87*, 230–235.
- (21) Directive 2013/39/EU of the European Parliament and of the Council of 12 August 2013 amending Directives 2000/60/EC and 2008/105/EC as regards priority substances in the field of water policy. *Off. J. Eur. Union* **2013**, *L 226*, 1-17.
- (22) Wesolowska, O.; Gąsiorowska, J.; Petrus, J.; Czarnik-Matusiewicz, B.; Michalak, K. Interaction of prenylated chalcones and flavanones from common hop with phosphatidylcholine model membranes. *Biochim. Biophys. Acta - Biomembr.* **2014**, *1838*, 173–184.
- (23) Ghazaryan, N. A.; Ghulikyan, L.; Kishmiryan, A.; Andreeva, T. V.; Utkin, Y. N.; Tsetlin, V. I.; Lomonte, B.; Ayyvazyan, N. M. Phospholipases A2 from Viperidae snakes: differences in membranotropic activity between enzymatically active toxin and its inactive isoforms. *Biochim. Biophys. Acta - Biomembr.* **2015**, *1848*, 463–468.

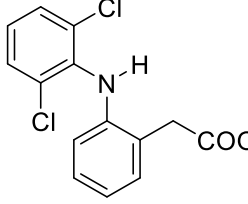
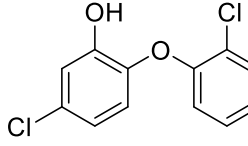


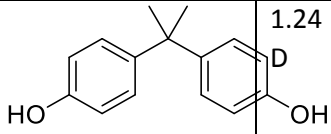
- (24) Kuźdżał, M.; Wesółowska, O.; Strancar, J.; Michalak, K. Fluorescence and ESR spectroscopy studies on the interaction of isoflavone genistein with biological and model membranes. *Chem. Phys. Lipids* **2011**, *164*, 283–291.
- (25) Vequi-Suplicy, C.C.; Benatti, C.R.; Lamy, M.T. Laurdan in fluid bilayer: position and structural sensitivity. *J. Fluoresc.* **2006**, *16*, 431-439.
- (26) Wu, D.-H.; Chen, A.; Johnson Jr, C.S. An improved diffusion-ordered spectroscopy experiment incorporating bipolar-gradient pulses. *J. Magn. Reson., Ser. A*, **1995**, *115*, 260-264.
- (27) Khajeh, A.; Modarress, H. Effect of cholesterol on behavior of 5-fluorouracil (5-FU) in a DMPC lipid bilayer, a molecular dynamics study. *Biophys. Chem.* **2014**, *187-188*, 43-50.
- (28) Lebecque, S.; Lins, L.; Dayan, F. E.; Fauconnier, M.-L.; Deleu, M. Interactions between natural herbicides and lipid bilayers mimicking the plant plasma membrane. *Front. Plant Sci.* **2019**, *10*, 329. DOI: 10.3389/fpls.2019.00329.
- (29) Viard, M.; Gallay, J.; Vincent, M.; Meyer, O.; Robert, B.; Paternostre, M. Laurdan solvatochromism: solvent dielectric relaxation and intramolecular excited-state reaction. *Biophys. J.* **1997**, *73*, 2221–2234.
- (30) Sachl, R.; Stepánek, M.; Procházka, K. Fluorescence study of the solvation of fluorescent probes prodan and laurdan in poly( $\epsilon$ -caprolactone)-block-poly(ethylene oxide) vesicles in aqueous solutions with tetrahydrofuran. *Langmuir* **2008**, *24*, 288-295
- (31) Suwalsky, M.; Manrique, M.; Villena, F.; Sotomayor, C.P. Structural effects in vitro of the anti-inflammatory drug diclofenac on human erythrocytes and molecular models of cell membranes. *Biophys. Chem.* **2009**, *141*, 34-40.
- (32) Oliver, M.; Bauzá, A.; Frontera, A.; Miró, M. Fluorescent lipid nanoparticles as biomembrane models for exploring emerging contaminant bioavailability supported by density functional theory calculations. *Environ. Sci. Technol.* **2016**, *50*, 7135-7143.
- (33) Lakowicz, J.R., Ed. *Principles of Fluorescence Spectroscopy*, 3rd, ed.; Springer Science + Business Media: New York, 2006.
- (34) Ma, J.C.; Dougherty D.A. The Cation- $\pi$  Interaction. *Chem. Rev.* **1997**, *97*, 1303-1324.
- (35) Malekar, S. A.; Sarode, A. L.; Bach II, A. C.; Worthen, D. R. The localization of phenolic compounds in liposomal bilayers and their effects on surface characteristics and colloidal stability. *AAPS Pharm. Sci. Tech.* **2016**, *17*, 1468-1476.
- (36) Wong-ekkabut, J.; Xu; Z.; Triampo W.; Tang I.-M.; Tieleman, D.P.; Monticelli, L. Effect of lipid peroxidation on the properties of lipid bilayer: a molecular dynamics study. *Biophys. J.* **2007**, *93*, 4225-4236.
- (37) Nagle, J. F.; Tristram-Nagle, S. Structure of lipid bilayers. *Biochem. Biophys. Acta* **2000**, *1469*, 159-195.

- (38) Martínez-Seara, H.; Róg, T. Molecular dynamics simulations of lipid bilayer: simple recipe of how to do it. In *Biomolecular Simulations: Methods and Protocols*; Monticelli, L.; Salonen, E., Eds.; Springer Science + Business Media: New York, Vol. 924, 2013, pp. 407-429.
- (39) Tabony, J.; Perly, B. Quasielastic neutron scattering measurements of fast local translational diffusion of lipid molecules in phospholipid bilayer. *Biochim. Biophys. Acta* **1990**, 1063, 67-72.
- (40) Almeida, P. F. F.; Vaz, W. L. C.; Thompson, T. E. Lateral diffusion in the liquid phases of dimyristoylphosphatidylcholine/cholesterol lipid bilayers: a free volume analysis. *Biochem.* **1992**, 31, 6739-6747.
- (41) Ferreira, H.; Lúcio, M.; Lima, J.L.F.C.; Matos, C.; Reis, S. Effects of diclofenac on EPC liposome membrane properties. *Anal. Bional. Chem.* **2005**, 382, 1256–1264.
- (42) Jurkiewicz, P.; Sýkora, J.; Olzyńska, A.; Humpolíckvá, J.; Hof, M. Solvent relaxation in phospholipid bilayers: principles and recent applications. *J. Fluoresc.* **2005**, 15, 883-894.
- (43) Jurkiewicz, P.; Cwiklik, L.; Jungwirth, P.; Hof, M. Lipid hydration and mobility: an interplay between fluorescence solvent relaxation experiments and molecular dynamics simulations. *Biochimie* **2012**, 94, 26-32.
- (44) Nitschke, W. K.; Vequi-Suplicy, C.C.; Coutinho, K.; Stassen, H. Molecular dynamics investigations of prodan in DLPC bilayer. *J. Phys. Chem. B* **2012**, 116, 2713-2721.
- (45) Chen, L.; Chen, J.-L.; Zhou, G.-Q.; Wang, Y.; Wang, X.-G. Molecular dynamics simulations of the permeation of bisphenol A and pore formation in a lipid membrane. *Sci. Rep.* **2016**, 6, 33399.

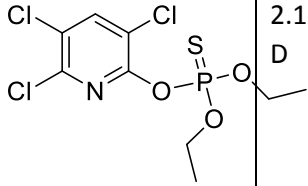
Table 1. Physicochemical properties of the target compounds including ecotoxicity data

Compound	formula	$\mu_D^{[b]}$	vdW volume <sup>[b]</sup>	logP <sup>[c]</sup> octanol/water	pKa	Microtox toxicity ( <i>Vibrio fischeri</i> )	Water flea toxicity ( <i>Daphnia sp.</i> )	Zebrafish toxicity ( <i>Danio rerio</i> )

<b>diclofenac</b> <sup>[a]</sup>		0.39 D (11.46 D)	323.4 Å <sup>3</sup> (324.3 Å <sup>3</sup> )	4.51 (log D=1.7)	4.1 5	73 μM IC <sub>50</sub> <sup>[d]</sup> at 15min <i>Environ. Pollut.</i> 237 (2018) 549  54 μM IC <sub>50</sub> at 15 min <i>Environ. Toxicol. Chem.</i> 36 (2017) 807	61 μM LC <sub>50</sub> <sup>[e]</sup> at 48h <i>Bull. Environ. Contam. Toxicol.</i> 97 (2016) 84	39 μM LC <sub>50</sub> at 48 hpf <sup>[f]</sup> <i>Sci. Total Environ.</i> 666 (2019) 1273
<b>triclosan</b>		1.25 D	295.2 Å <sup>3</sup>	4.76	7.9	2.5 μM IC <sub>50</sub> at 15 min <i>Chemosphere</i> 108 (2014) 239	1.1 μM LC <sub>50</sub> at 48h <i>Ecotoxicol. Environ. Sci.</i> 22 (2013) 1384  2.1 μM LC <sub>50</sub> at 48h <i>Environ. Sci. Pollut. Res.</i> 26 (2019) 16289	2.2 μM LC <sub>50</sub> at 48 hpf <i>Environ. Sci. Technol.</i> 53 (2019) 11988  3.9 μM LC <sub>50</sub> at 48 hpf <i>Sci. Total Environ.</i> 666 (2019) 1273

bisphenol A		1.24	296.5 Å <sup>3</sup>	3.32	9.6	27 μM IC <sub>50</sub> at 15min <i>Comp. Biochem. Physiol. C</i> , 152 (2010) 407	64 μM LC <sub>50</sub> at 48h <i>Environ. Sci. Pollut. Res.</i> 24 (2017) 23872	63 μM LC <sub>50</sub> at 48 hpf <i>Sci. Total Environ.</i> 666 (2019) 1273
						38 μM IC <sub>50</sub> at 30min <i>Molecules</i> 23 (2018) 3226	56 μM LC <sub>50</sub> at 48h <i>J. Health Sci.</i> 50 (2004) 97	

Journal Pre-proof

chlorpyrifos		2.19 D	357.7 Å <sup>3</sup>	4.96	-	0.76 μM IC <sub>50</sub> at 15min <i>J. Hazard. Mat. B103 (2003) 93</i>	2.3×10 <sup>-4</sup> μM LC <sub>50</sub> at 48h <i>Environ. Toxicol. Chem. 33 (2014) 1337</i>	16 μM LC <sub>50</sub> at 5 dpf <sup>[g]</sup> <i>Environ. Toxicol. Chem. 33 (2014) 1337</i>
							2.6×10 <sup>-4</sup> μM LC <sub>50</sub> at 48h. <i>J. Ecotox. Environ. Safety 71 (2008) 219</i>	3.4 μM LC <sub>50</sub> at 99 hpf <i>J. Hazard. Mater. 334 (2017) 121</i>
							1.4×10 <sup>-3</sup> μM LC <sub>50</sub> at 48h <i>Ecotox. Environ. Safety 64 (2006) 207</i>	2.0 μM LC <sub>50</sub> at 96 h in adult <i>Environ. Toxicol. Pharma col. 43 (2016) 166</i>

[a] Values in parenthesis correspond to the anionic form of the carboxylic group.

[b] The dipole moment and the van der Waals (vdW) volume values were estimated using density functional theory (DFT) calculations at the B3LYP/6-31G\* level of theory using the Spartan'10 v.1.0 program (Wavefunction INC. 18401 von Karman Ave., Irvine, CA 92612. www.wavefun.com).

[c] Experimental values (www.chemspider.com)

[d] IC<sub>50</sub>: median inhibition concentration

[e] LC<sub>50</sub>: median lethal concentration

[f] hpf (hours post fertilization)

[g] dpf (days post fertilization)

**Table 2.** Average area per lipid ( $A_{PLPC}$ ), average thickness (h) of the

lipid bilayer and the lateral diffusion coefficient of the bilayer ( $D_{lat}$ ) for each of the four contaminants and the membrane probes.

Compound	$A_{PLPC}$ (nm <sup>2</sup> )	h (nm)	$D_{lat}$ PLPC (cm <sup>2</sup> /s)
Laurdan	0.649±0.002	3.74	$(9.2±6.0) \times 10^{-8}$
Prodan	0.645±0.005	3.64	$(10.7±6.7) \times 10^{-8}$
Chlorpyrifos	0.659±0.003	3.75	$(5.9±2.0) \times 10^{-8}$
Triclosan	0.658±0.004	3.73	$(7.4±5.6) \times 10^{-8}$
Bisphenol A	0.657±0.005	3.72	$(8.0±1.0) \times 10^{-8}$
Diclofenac	0.659±0.002	3.70	$(19.2±12.2) \times 10^{-8}$

#### CONFLICT OF INTEREST

The authors declare that there is no conflict of interest to disclose

#### Credit Author Statement

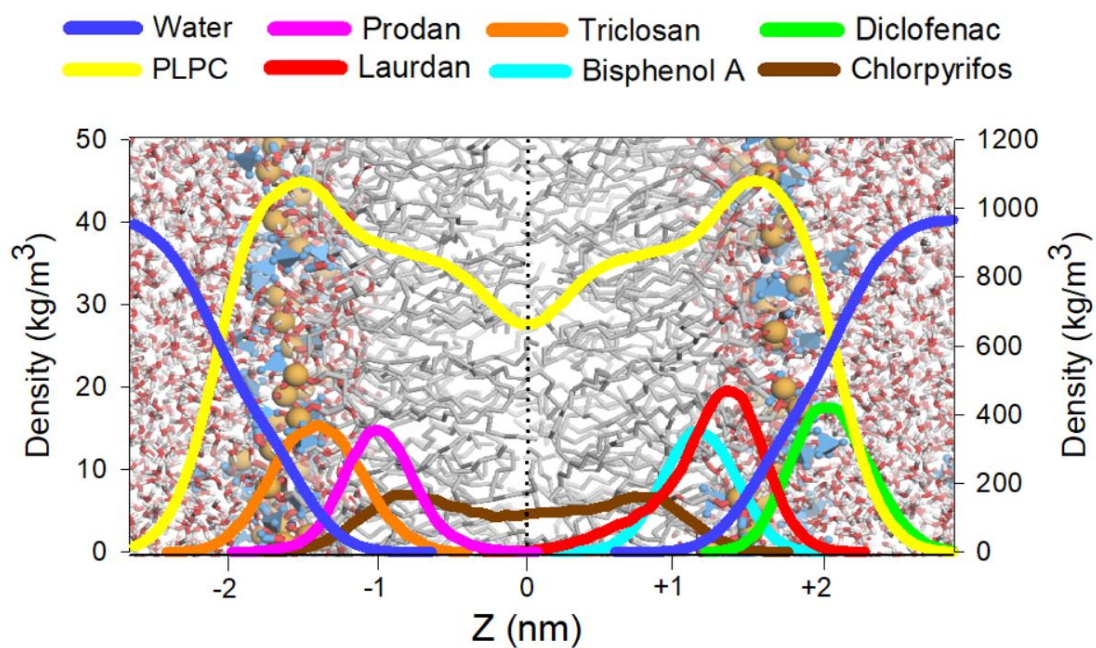
Miquel Oliver: Investigation; Methodology; Validation; Visualization; Formal Analysis; Writing - Original Draft

Miquel Adrover: Conceptualization; Methodology; Investigation; Visualization; Formal Analysis; Resources; Writing - Review & Editing

Antonio Frontera: Conceptualization; Methodology; Formal Analysis; Writing - Review & Editing

Joaquín Ortega-Castro: Conceptualization; Methodology; Investigation; Visualization; Formal Analysis; Resources; Writing - Review & Editing

Manuel Miró: Conceptualization; Methodology; Supervision; Funding acquisition; Project administration; Resources; Writing - Review & Editing



### Highlights

Liposomes as models for *in-vitro* investigation of contaminant bioavailability

Multidisciplinary approach based on fluorescence and NMR data and molecular dynamics

Application to emerging organic pollutants with different physicochemical properties

Fluorescent probes for fast insight into contaminant permeation across lipid bilayers